Title

Breathing Chest Radiography using a Dynamic Flat-Panel Detector (FPD) Combined with Computer Analysis

The type of manuscript

Research Article

Authors

Rie Tanaka*, Shigeru Sanada*, Masayuki Suzuki*, Takeshi Kobayashi**, Takeshi Matsui**, Hitoshi Inoue***, Yoshihisa Nakano****

* Department of Radiological Technology, School of Health Sciences, Kanazawa University;

** Department of Radiology, Kanazawa University Hospital; 13-1 Takaramachi, Kanazawa, Japan

*** DR Systems Development Dept.5, CANON INC; 20-2 Utsunomiya, Japan

**** Department of Radiology, Kyoto Katsura Hospital; 17 Hirao, Yamada, Nishikyouku, Kyoto, Japan

Information concerning grants

This work was partially supported by a Grant-in-Aid for Science, Japan, and by a grant from CANON INC.

Address for reprint requests

Rie Tanaka, MS.

Sanada Lab, Department of Radiological Technology, School of Health Sciences, Faculty of Medicine, Kanazawa University;

5-11-80 Kodatsuno, Kanazawa, 920-0942, Japan

Abstract

Kinetic information is crucial when evaluating certain pulmonary diseases. When a dynamic Flat-Panel Detector (FPD) can be used for a chest examination, kinetic information can be obtained simply and cost-effectively. The purpose of this study was to develop methods for analyzing respiratory kinetics, such as movement of the diaphragm and lung structures, and the respiratory changes in X-ray translucency in local lung fields. Postero-anterior dynamic chest radiographs during respiration were obtained with a modified FPD, which provided dynamic chest radiographs at a rate of 3 frames per second. Image registration for correction of physical motion was followed by measurement of the distance from the lung apex to the diaphragm. Next, we used a cross-correlation technique to measure the vectors of respiratory movement in specific lung areas. Finally, the average pixel value for a given local area was calculated by tracing the same local area in the lung field. This method of analysis was used for six healthy volunteers and one emphysema patient. The results reported here represent the initial stage in the development of a method that may constitute a new method for diagnosing certain pulmonary diseases, such as chronic obstructive pulmonary disease, fibroid lung, and pneumonia. A clinical evaluation of our method is now in progress.

Key words:

Chest radiography, Flat-panel detector, Respiratory kinetics

Introduction

Pulmonary diseases are increasing worldwide against a background of an aging society, worsening air pollution, and widespread cigarette smoking. For example, chronic obstructive pulmonary disease (COPD) occupies fourth place in causes of death in the United States, and eighth place in Japan.[1, 2] COPD occurs primarily in the elderly and needs long-term treatment; thus, a means to control this disease at low cost is urgently needed. One potential tool for managing pulmonary disease is chest radiography using large field dynamic flat-panel detectors (FPDs). With these devices, it is now possible to obtain dynamic chest radiographs during respiration. Dynamic chest radiography could provide several benefits. First, it could provide information about the movement of the diaphragm and lung regions, making it possible to evaluate the function of each lung separately. Second, it could measure reductions in diaphragmatic excursion, which are associated with pulmonary diseases such as phrenic nerve numbness and restrictive pulmonary disease. Third, it could be used to evaluate patients considering lung volume reduction surgery (LVRS) and monitor their postoperative recovery. For example, a patient with bulla but without reduction of diaphragmatic excursion is considered contraindicative for LVRS, because the aim of LVRS is to restore diaphragmatic movement. Fourth, it can detect changes in X-ray translucency during respiration, which are related to the level of air ventilation -- areas with decreased ventilation may be bullous or fibrotic. For these reasons, we have embarked upon the development of an imaging technique using a dynamic FPD and a computerized system for quantitative analysis of respiratory kinetics on dynamic chest radiographs.

Many investigators have tried to obtain data on respiratory kinetics using conventional methods, involving various kinds of image-based examinations. Kymography is a conventional method for obtaining two-dimensional kinetic information.[3, 4] This type of radiography did not come into general clinical use due to the development of other diagnostic examinations. Chest radiography using a large-field image intensifier (I.I.) was also tested for use in clinical practice.[5, 6] The usefulness of this approach has been suggested in several reports, but it has not been

adopted for clinical use because of distortion in the I.I., its low spatial resolution and the presence of large amounts of veiling glare and structural mottle.[7] On the other hand, with a three-dimensional approach to kinetic information, dynamic MRI can provide respiratory functional data about the diaphragm and the rib cage.[8, 9] Dynamic CT can also be used for analyzing respiratory changes in local lung CT values and movement of lung masses.[10, 11] These respiratory kinetic data are reportedly useful for diagnosing COPD, for making decisions pertaining to LVRS, and for observing postoperative progress. Investigators have reported on the use of dynamic CT for the assessment of invasion of lung cancer into the mediastinum and chest wall.[12-15] However, none of these diagnostic approaches has come into practical use because of low-level throughput and poor cost performance. However, when a dynamic FPD is used for chest examination, the kinetic information can be obtained simply and cost-effectively. In this study, we investigated methods for analyzing the movement of the diaphragm, the movement of structures within the lung, and respiratory changes in x-ray translucency. This study therefore represents the initial stage in the development of a potential new method for diagnosing pulmonary diseases.

Materials and Methods

Data Acquisition

Fluoroscopic posteroanterior (PA) chest images of six healthy volunteers and a patient with emphysema during respiration were obtained with a modified FPD (CXDI-22, Canon Co., Ltd., Tokyo, Japan). The exposures were taken at 120 kV, 80 mA, 3.2 msec, and 3 frames per second, and source image distance (SID) was 2.0 m. The total number of frames was 30 frames over 10 seconds. The matrix size was 2688 x 2688 pixels, the pixel size was 160 μm, and the gray-level range of the images was 4096. The entrance surface dose, measured in air without backscattering, was approximately 0.4 mGy, which was 150% of that obtained with conventional PA chest radiography using a Fuji Computed Radiography system (Fuji Medical Systems Co., Ltd., Tokyo, Japan) at our hospital. For this study, approval by the institutional review board and informed consent from the patient were obtained. An experienced radiologist confirmed that the chest radiographs of the volunteers were normal. The patient with emphysema was diagnosed by CT examination and respiratory functional test.

Image Analysis

Analysis was performed on a personal computer (Operating system: Windows 2000 ; Microsoft, USA) with software developed by us (Development environment: C++Builder ; Borland, Scotts Valley, USA).

(1) Image registration and recognition of lung area

The overall schema of our analysis is illustrated in Fig. 1. First, image registration for the correction of physical motion was performed in cases with physical motion. The rib cage edges were detected by using the first derivative of the horizontal image profile at three different levels, after which the center vertical lines were determined through all frames. Dynamic chest radiographs after the second frame were then shifted or rotated to match the center vertical lines with the one of the first frame. Second, the lung area was determined by means of edge detection using

the first derivative technique and iterative contour-smoothing algorithm shown in Fig. 2(a).[16, 17] Since the edges of the heart or gas in the stomach often interfere with detection of the left hemidiaphragm edge, the more reliably identifiable right hemidiaphragm edge is used as an index to determine the left hemidiaphragm, which, however, may be adversely affected by an abnormal right hemidiaphragm. The overall success rate for automatic lung recognition was 60 %. Some cases showed errors, which was mainly due to the lack of a part of the lung area, so that manual corrections were needed for some frames after the automatic detection. Therefore, when a result of the automated lung detection was judged to be incorrect by a chest radiologist, we corrected it manually.

(2) Measurement of diaphragmatic movement

The position of the hemidiaphragm and the lung apex was determined as shown in Fig. 2(a)-(b), after which the distance from the lung apex to the hemidiaphragm was measured as shown in Fig. 2(c). Dynamic chest radiographs were processed with a 7 x 7 Sobel filter to produce images with an enhanced edge. The points for measurement decided in the first frame were traced after the second frame with the aid of the sequential similarity detection algorithm (SSDA) using the ROI in the previous frame as a template as shown in Fig. 2(d). The template was renewed every frame, so that accurate tracking was readily achieved.[18] The measured distance was also used to determine the respiratory phase as shown in Fig. 3. Because the movement of the diaphragm directly reflects the respiratory phase[19], the respiratory phase was assumed from the change in the distance.

(3) Analysis of lung structures' movement

We measured the vectors of respiratory movement in all local lung areas using a cross-correlation technique.[20] The local area (100 x 100 pixels) in the frame being examined was searched for the most similar local area in the previous frame. The size of the local area was chosen to approximate the size of the intercostal space, since the ribs are a major source of anatomical structure in the chest.[21] The size of the search

area was 164 x 220 pixels, because of the respiratory property that the movement of lung structures along the cephalocaudal axis is more extensive than along the horizontal axis. The difference (D) between the previous local area, $f_{n-1}(x_i+dx, y_j+dy)$, and the one being examined, $f_n(x_i, y_j)$, was expressed as follows:

$$D = \sum_j \sum_i \left| f_n(x_i, y_j) - f_{n-1}(x_i + dx, y_j + dy) \right| \qquad (1)$$

$$-32 \le dx < 32, \quad -60 \le dy < 60, \quad 1 \le n < 30,$$

$$0 \le i < 100, \quad 0 \le j < 100$$

This means that the smaller D is, the more similar the two local areas in the frame being examined and in the previous frame are. Assuming that the center coordinate of the square local area in the frame being examined is [xe, ye] and that of the previous frame is [xs, ys], the vector [vx, vy] is [(xe-xs), (ye-ys)]. Respiratory vectors from the previous frame to the frame being examined were superimposed on the coordinates of the latter, as shown in Fig. 4. The relationship between the respiratory phase and the average magnitude of the vectors of movement in lung segmentation was then analyzed. We divided each lung into three lung fields of equal area (upper, middle, and lower) based on the number of pixels. For comparison of lung fields, the average magnitude of the vector movement was obtained by dividing the sum of movement magnitudes by the number of measurement points in a given lung field.

(4) Analysis of the respiratory changes in average pixel values in local areas

To examine the changes in pixel values, we manually located four regions of interest (ROIs) on the upper and the lower lung fields in both lungs (Fig. 5a). For accurate comparison among subjects, ROIs were placed in approximately the same anatomic position in each subject. One side of the ROI was 100 pixels long, which was about the same size as the intercostal space. The ROIs tracked the same local area during respiration in the lung field and the average pixel value for a given ROI was calculated by dividing total pixel values by the total number of pixels in that ROI. The relationship between the respiratory phase and average pixel value for the ROI was analyzed for one healthy volunteer and one emphysema patient by calculating the

correlation coefficient [$r = \sum (x - \bar{x})(y - \bar{y}) / \sqrt{\sum (x - \bar{x})^2 \sum (y - \bar{y})^2}$], where x is the lung apex-diaphragm distance and y is the average pixel value within an ROI. The relationship of average pixel value for the right and left ROI was also analyzed by calculating the correlation coefficient [$r = \sum (ry - \overline{ry})(ly - \overline{ly}) / \sqrt{\sum (ry - \overline{ry})^2 \sum (ly - \overline{ly})^2}$], where ry is the average pixel value within a right ROI and ly is that within a left ROI. For all of the patients, we also measured how much the average pixel value within an ROI (y) changed during the respiratory cycle. This was accomplished by calculating the difference between the maximum value of y and the minimum value of y over the respiratory cycle. We refer to this difference as the translucency change. The results were compared for the healthy volunteers and the emphysema patient. Since we hypothesize that the lung regions have different translucency changes, we also computed the Wilcoxon test statistic, using the upper lung regions as one group and the lower lung regions as the second group.

Low pixel values were related to dark areas in the images and this in turn was related to a high X-ray translucency in this system. The pixel value was inversely proportional to the logarithm of the incident exposure into the FPD. When the difference between the maximum and minimum average pixel values during the respiratory cycle in a certain area is twice that in another area, it means that the variation of logarithm of relative exposure is twice as great.

Results

(1) Analysis of lung structures' movement

Sequential chest radiographs with local vectors from the preceding frame to the frame being examined are shown in Figs. 4(a)-(c). The arrows indicate the orientation and magnitude of the movement from the previous frame. Figure 4(b) shows the inspiratory phase and Fig. 4(c) the expiratory phase. The results make it possible to understand the orientation and magnitude of the movement in quantitative terms. In this example, the lung vectors in the inspiratory phase tended to be oriented downwards and the vectors in the expiratory phase tended to be oriented upwards. However, the vectors on the ribs during expiration (Fig. 4c) are pointing downwards or to the right, whereas the vectors on the diaphragm and a few of the vectors in the lung field are pointing upwards.

Figure 6 shows the changes in the average magnitude of the respiratory vectors in all lung fields. The respiratory phase was determined from the diaphragm movement shown in Fig. 3. These graphs clearly show that the movement of the lung markings of the lower lung field was larger than that of the upper lung field in both lungs during both inspiration and expiration. There were no remarkable differences between the right and the left lung fields at the same cephalocaudal level.

(2) Analysis of the respiratory changes in average pixel values in local areas

Figure 5 shows the results for a healthy volunteer. Figures 5(b) and 5(c) show the relationship between frame number and the average pixel value in the ROIs shown in Fig. 5(a). The distance from the lung apex to the diaphragm was used as an effective and simple index of the respiratory phase.

Average pixel values tended to decrease in the inspiratory phase but tended to increase in the expiratory phase as shown in Figs. 5(b)-(c). This tendency was observed in all of the subjects. The difference in average pixel values between the right and left lung shown in Fig. 5(b) and (c) is caused by the difference in the portion of the rib area included in the ROI. Our results indicate that the average pixel value in the right lung changes in synchronization with that in the left lung (Upper: r=0.94;

lower: r=0.96). The average pixel value within an ROI changes regularly in synchronization with the respiratory phase estimated from the level of the diaphragm (Upper right: r=-0.90; upper left: r=-0.95; lower right: r=-0.93; lower left: r=-0.96). The variation between a value at one given time and the value at the next time is shown in Fig. 5(d) and Fig. 5(e), which also show this synchronization. The correlation was negative since the pixel value was inversely proportional to the logarithm of the incident exposure into the FPD.

Figure 7 shows the results for the emphysema patient. In the upper lung fields, the difference between average pixel values of the ROIs in the two lungs was less than 50 (pixel value) during any respiratory phase (Fig. 7b). In the lower lung field, however, the gradient of change in average pixel value in the left lung field with trapped air was clearly more gentle than in the right lung field (Fig. 7c). Furthermore, average pixel values do not follow the diaphragmatic movement as closely as those of the healthy volunteer except for the right lower lung field (Upper right: r=-0.80; upper left: r=-0.66, lower right: r=-0.99; lower left: r=-0.82). Figures 7(d) and (e) show that the synchronization between the average pixel value in the lung ROIs and the movement of the diaphragm decreased except for the right lower lung field.

Figures 8(a)-(c) show the difference between the maximum and minimum average pixel values during the respiratory cycle in the upper and lower lung fields. In healthy volunteers, no significant difference was seen between the right and left lungs as shown in Figs. 8(a) and (b). However, the difference in average pixel values in the upper lung field was less than that in the lower lung field ($p < 0.01$) as seen in Fig. 8(c). These results confirmed the rule that, as the air volume in the lung increases, the X-ray translucency also increases. On the other hand, in the emphysema patient, the difference in average pixel values in the left lower lung field with trapped air was only half of that in the right lower lung field. However, on an individual level differences could be found for case #. 4 in Fig. 8b. Thus, it is necessary to accumulate respiratory data to establish the criterion for abnormal respiratory kinetics.

Discussion

For measuring diaphragmatic movement, the distance from the lung apex to the diaphragm could be measured automatically and the results were used as an index of the respiratory phase for analysis of both respiratory movement and of respiratory changes in average pixel values in local areas. The clinical usefulness of image based kinetic information regarding diaphragmatic movement has been reported by many investigators.[8-9] However, their dynamic images were obtained with dynamic MRI and the measurements were performed manually, resulting in high cost and requiring a long time. In contrast, imaging with dynamic FPD combined with our computer analysis is expected to take only a few minutes. However, it is need to improve the accuracy of automatic recognition of lung area throughout all frames, because our methods dose not always provide complete lung recognition at present stage.

For the analysis of respiratory movement, our method made it possible to measure the orientation and magnitude of movement in the lung fields. This method was developed with a view to detecting irregular movements of lung vessels caused by abnormal surroundings. However, the vectors obtained with our results could not show the movement of lung vessels only because of noise, which caused movement in different directions on the projected images. This is because lung markings for faint shadows were washed out by the clear shadows of the ribs and heart. The impact of this effect on our results in terms of the detection of abnormal movements cannot be ignored. For example, the shadows of lung vessels invading into the pleura are thought to move less than those of normal lung vessels, so that resulting errors would interfere with detection of this kind of abnormality. We are now exploring ways to improve the accuracy of vector measurement for lung markings. We think that elimination of the shadows of the ribs by means of sequential dual-energy subtraction technique using dynamic FPD is one of the solutions for this problem.

The analysis of the respiratory changes in average pixel values showed that our results were consistent with well-known characteristics observed during respiration. The respiratory change in X-ray translucency depends on how close the lung markings are clustered together.[22] Our results changed predictably due to the change in X-ray

translucency resulting from the respiratory phase. The results of all healthy volunteers showed the normal pattern of respiratory physiology, where pixel values decrease during inspiration and increase during expiration. In addition, no remarkable differences were seen in the changes in local pixel values between the two lungs. On the other hand, analysis of the emphysema patient showed a large difference in the process of change in the lower lung field of the right and left lung, although the left diaphragm moved as dynamically as the right diaphragm. Furthermore, there was a remarkable reduction in the difference between the maximum and minimum average pixel values in the left lower lung field during the respiratory cycle. Such a reduction seen on dynamic chest radiographs would be due to a large amount of trapped air which was confirmed on the CT image. These results suggest that our method may constitute a new way to detect trapped air on dynamic chest radiographs. However, since only one case of emphysema and six healthy volunteers were analyzed in this study, a larger number of subjects is needed to confirm the usefulness of this method in clinical practice.

Our method is advantageous both in terms of cost and time. For example, dynamic chest radiographs during respiration can be obtained in 10 seconds with the same positioning as used for conventional chest radiography. Moreover, radiologists can observe dynamic images on the monitor without the need for film. When the functional test with a spirometer is used as a form of noninvasive examination, it cannot provide information about the function of each lung separately. The main merit of our dynamic study is therefore that it can evaluate the function of each lung separately and use the images to analyze the process of change, from inspiration to expiration. Furthermore, it should be noted that the absorbed dose with our method is up to 1.5 times that of conventional PA chest radiography using an FCR system employed at our hospital.

However, our method is of limited accuracy because dynamic chest radiographs are two-dimensional projections. Further, one-third of the lung vessels and bronchi from the hilum of the lung are rarely visualized on radiographs.[23] Thus, these images cannot be used to analyze the peripheral lung markings and the pulmonary alveoli. It

is also true, however, that major variations are seen within healthy volunteers, partly caused by breathing during imaging. There is also an urgent need to establish an imaging protocol for retaining reproducibility of the results, which we plan to deal with in the future.

In terms of pathologic physiology, the most important targets for this examination are COPD, restrictive pulmonary disease, phrenic nerve numbness, and pulmonary edema. In clinical trials now in progress, the results obtained with our method have been useful in some cases. For diagnosis of the fibroid lung, the measurement of the movement of the diaphragm and chest wall proved that, due to advanced fibrosis, the patient could not perform abdominal respiration, which is achieved with the diaphragm, but could perform thoracic respiration, which is achieved with the chest wall and costal muscle. A reduction in the changes in local average pixel values was also observed. For the analysis of interstitial pneumonia in a postoperative right lung, the results showed that the function of the right lung was still inferior to that of the left lung in terms of diaphragmatic movement. Such evaluations would not be possible from the basis of findings on static images and the results of the respiratory functional test. Furthermore, our method was very effective in a case of a bronchial asthma whose respiratory function could not be examined with the respiratory functional test due to the condition of the postoperative larynx.

Although this study may be useful for diagnosis based on chest examination results, there is not enough clinical evidence to confirm its diagnostic effectiveness. Therefore, we need (1) to analyze many types of abnormal subjects, (2) to accumulate many quantified respiratory data, (3) to compare the diagnostic capability of our method with that of other examination techniques, and (4) to identify and clarify the respiratory kinetics for each disease.

In this study, we developed a method for quantifying respiratory kinetics on dynamic chest radiographs, and the analysis of the findings was applied to six healthy volunteers and one case of emphysema. We demonstrated that our method could quantify respiratory kinetics and the properties thereof for the dynamic chest. In conclusion, our imaging technique and our method for quantitative kinetic analysis of

dynamic chest images can easily provide additional diagnostic information, which could not be obtained with conventional methods. Demonstrating its usefulness is an issue for the future studies. Our eventual goal is to develop a computer-aided diagnostic system that provides total respiratory kinetic information for chest examinations.

Acknowledgments

This work was partially supported by Canon Inc., Tateishi Science and Technology Foundation, and a Grant-in-Aid from the Japanese Ministry of Education, Culture, Sports, Science and Technology. The authors are grateful to the volunteers who assisted with the data acquisition and to Steve Leary for improving the manuscript.

References

[1] National Vital Statistics Report., *National Center for Health Statistics*, Maryland, Washington DC, **49**, 1-40 (2001).

[2] "ATS statement: Standards for the Diagnosis and Care of Patients with Chronic Obstructive Pulmonary Disease," Am J Respir Crit Care Med. **152**, S77-S120 (1995).

[3] V. Gall, "Strip Kymography of the Glottis," Arch Otorhinolaryngol. 240, 287-293 (1984).

[4] M. Tigges, P. Wittenberg, P. Mergell, and U. Eysholdt, "Imaging of vocal fold vibration by digital multi-plane kymography," Comput Med Imaging Graph. **23**, 323-330 (1999).

[5] H. Manninen, K. Partanen, S. Soimakallio, and H. Rytkonen, "Image-intensifier photofluorography and conventional radiography: comparison of diagnostic efficancy," AJR Am Roentgenol. **150**, 539-544 (1988).

[6] K.L. Lam, H.P. Chan, H. MacMahon, W.T. Oravecz, K. Doi, "Dynamic digital subtraction evaluation of regional pulmonary ventilation with nonradioactive xenon," Invest Radiolo. **25**, 728-735 (1990).

[7] H. Fujita, K. Doi, H. MacMahon, Y. Kume, M. L. Giger, and K. R. Hoffmann, "Basic imaging properties of a large image intensifier-TV digital chest radiographic system," Invest Radiol. 22, 328-335 (1987).

[8] K. Suga, T. Tsukuda, H. Awaya, K. Takano, S. Koike, N. Matsunaga, K. Sugi, and K. Esato, "Impaired Respiratory Mechanics in Pulmonary Emphysema. Evaluation with Dynamic Breathing MRI," JMRI. **10,** 510-520 (1999).

[9] O. Unal, H. Arslan, K. Uzun, B. Ozbay, M. E. Sakarya, "Evaluation of diaphragmatic movement with MR fluoroscopy in chronic obstructive pulmonary disease," Clin Imaging. **24**(6), 347-350 (2000).

[10] W. R. Webb, J. E. Stern, N. Kanth and G. Gamsu, "Dynamic Pulmonary CT: Findings in Healthy Adult Men," Radiology. **186,** 117-124 (1993).

[11] M. David, U. Athol, B. Michael and J. Peter, "Bronchiectasis: Functional Significance of Areas of Decreased Attenuation at Expiratory CT," Radiology. **193**,

369-374 (1994).

[12] K. Murata, M. Takahashi, M. Mori, K. Shimoyama, A. Mishina, S. Fujino, H. Itoh, and R. Morita, "Chest Wall and Mediastinal Invasion by Lung Cancer: Evaluation with Multisection Expiratory Dynamic CT," Radiology. **191,** 251-255 (1994).

[13] T. Shirakawa, K. Fukuda, Y. Miyamoto, H. Tanabe and S. Tada, "Parietal Pleural Invasion of Lung Masses: Evaluation with CT Performed During Deep Inspiration and Expiration," Radiology. **192,** 809-811 (1994).

[14] J. D. Mace, N. Kowalczyk, *Radiographic Pathology for Technologists*, 2nd ed. St. Louis, MO, Mosby, 91-94 (1994).

[15] S. Sakai, S. Murayama, J. Murakami, N. Hashiguchi and K. Masuda, "Bronchogenic Carcinoma Invasion of the Chest Wall," J Comput Assist Tomogr. **21,** 595-600 (1997).

[16] X. W. Xu, K. Doi, "Image Feature Analysis for Computer-Aided Diagnosis: Accurate Determination of Ribcage Boundary in Chest Radiographs," Med Phys. **22**, 617-626 (1995).

[17] L. Li, Y. Zheng, M. Kallergi and R. A. Clark, "Improved Method for Automatic Identification of Lung Regions on Chest Radiographs," Acad Radiol. **8**, 629-638 (2001).

[18] D. I. Barnea, H. F. Silverman, "A Class of Algorithms for Fast Digital Image Registration", IEEE Trans. Comput. **c-21**, 179-186 (1972).

[19] J. B. West, Mechanics of breathing. In: *Respiratory Physiology* – the essentials 5th ed. (Williams & Wilkins, Baltimore, Philadelphia, Hong Kong, London, Munich, Sydney, Tokyo, 1995), pp. 89-116.

[20] H. Dana and M. Christopher, Early processing. In: *Computer Vision*, (Englewood Cliffs, New Jersey: Prentice-Hall, 1982), pp. 107-109.

[21] A. Kano, K. Doi, H. MacMahon, D. Hassel, D. Dayne and M. L. Giger, "Digital Image Subtraction of Temporally Sequential Chest Images for Detection of Interval Change," Med Phys. **21**, 453-461 (1994).

[22] L. F. Squire and R. A. Novelline, Overexpansion and Collapse of the Lung. In: *Fundamentals of Radiology*, 4th ed. (Cambridge, Massachusetts, and London,

England: Harvard University Press, 1988), pp. 88-89.

[23] B. Felson, Chap.5 The hila and pulmonary vessels. In: Chest Roentgenology, (Philadelphia, London, and Toront: W .B. Saunders company, 1973), pp. 185-213.

Legends for illustrations

Fig. 1 Overall schema of our analysis technique.

Fig. 2 The lung area was determined by means of edge detection using the first derivative technique and iterative contour-smoothing algorithm. The image demonstrates the detection of the points of the hemidiaphragm and the lung apex used for measuring diaphragmatic movement. (a) ① Hatched area shows the area of analysis for a horizontal signature across a 1/8 section near the middle of the image. Circles represent rib cage edge and mediastinum edge locations as estimated from the first derivatives of the horizontal signature. ② Hatched areas show the area of analysis for vertical signatures across a 1/8 section on the midpoint between the rib cage edge and the mediastinum edge. Triangles represent the hemidiaphragmatic edge locations as estimated from the first derivatives of the vertical signature. (b) The position of the lung apex is determined as the highest point between the broken vertical line and the solid vertical line. Squares represent the lung apex edge locations. (c) Measurement place of the distance from the lung apex to the hemidiaphragm. (d) The points on the lung apex and the hemidiaphragm are traced with the Sequential Similarity Detection Algorithm (SSDA) technique after the second frame. Solid rectangles represent ROIs and dotted rectangles the search areas. The size of ROIs is 100 x 100 for the lung apex and 100 x 120 for the diaphragm, and that of the search areas is 120 x 120 for the lung apex and 120 x 320 for the diaphragm.

Fig. 3 This graph shows the result of measuring movement of the right hemidiaphragm. Hemidiaphragm movement based on the distance was used as an index of the respiratory phase. When the distance from the lung apex to the diaphragm increased, respiration was assumed to be the inspiratory phase, and when the distance decreased, it was assumed to be the expiratory phase. The subject is #5 in Fig. 8.

Fig. 4 (a) Sequential images with local vectors. The small arrows represent local

vectors indicating the orientation and magnitude of the movement from the previous frame. The area enclosed by the square in Fig. 4(a) is shown enlarged in (b) at the beginning of inspiration from frame # 6 to frame # 7, and (c) halfway during expiration from frame # 26 to frame # 27.

Fig. 5 Relationship between respiratory phase and average pixel value in the local lung field: healthy volunteer. (a) Squares indicate ROIs for the measurement of average pixel values in local areas. Average pixel value curves for (b) the upper lung field and (c) the lower lung field. The distance from the lung apex to the diaphragm was used as an index of the respiratory phase. Difference bar graphs for (d) the upper lung field and (e) the lower lung field in the right lung. The subject is # 4 in Fig. 8.

Fig. 6 Averaged vector curves for (a) the upper, (b) the middle, and (c) the lower lung fields. The data is the average for one case. The diaphragmatic movement of the subject is demonstrated in Fig. 3. The average size of the movement vector in the upper lung field was nearly constant regardless of respiratory phase. In the middle and lower lung fields, changes in the average size of movement correspond to the respiratory phase.

Fig. 7 Relationship between respiratory phase and average pixel values in the local lung field: emphysema with large amount of trapped air in the lower lung field. (a) Squares indicate ROIs for the measurement of average pixel values in local areas. Trapped air can be identified in the left lower lung field. Average pixel value curves for (b) the upper lung field and (c) the lower lung field. The distance from the lung apex to the diaphragm was used as an index of the respiratory phase. Difference bar graphs for (d) the upper lung field and (e) the lower lung field in the right lung.

Fig. 8 Differences in the maximum and minimum average pixel values during a respiratory cycle for six healthy volunteers and one emphysema patient in (a) the upper lung field and (b) the lower lung field. Four additional measurements were performed

in the four squares around each ROI as shown in the insert. The error bars indicate ± 1SD of the difference between the maximum and minimum average pixel values during a respiratory phase for all five squares (= the ROI and the four squares around the ROI). (c) Comparison of the average differences between the upper and lower lung fields in six healthy volunteers. Case # 4 is shown in Fig. 6 and case # 5 in Fig. 3.

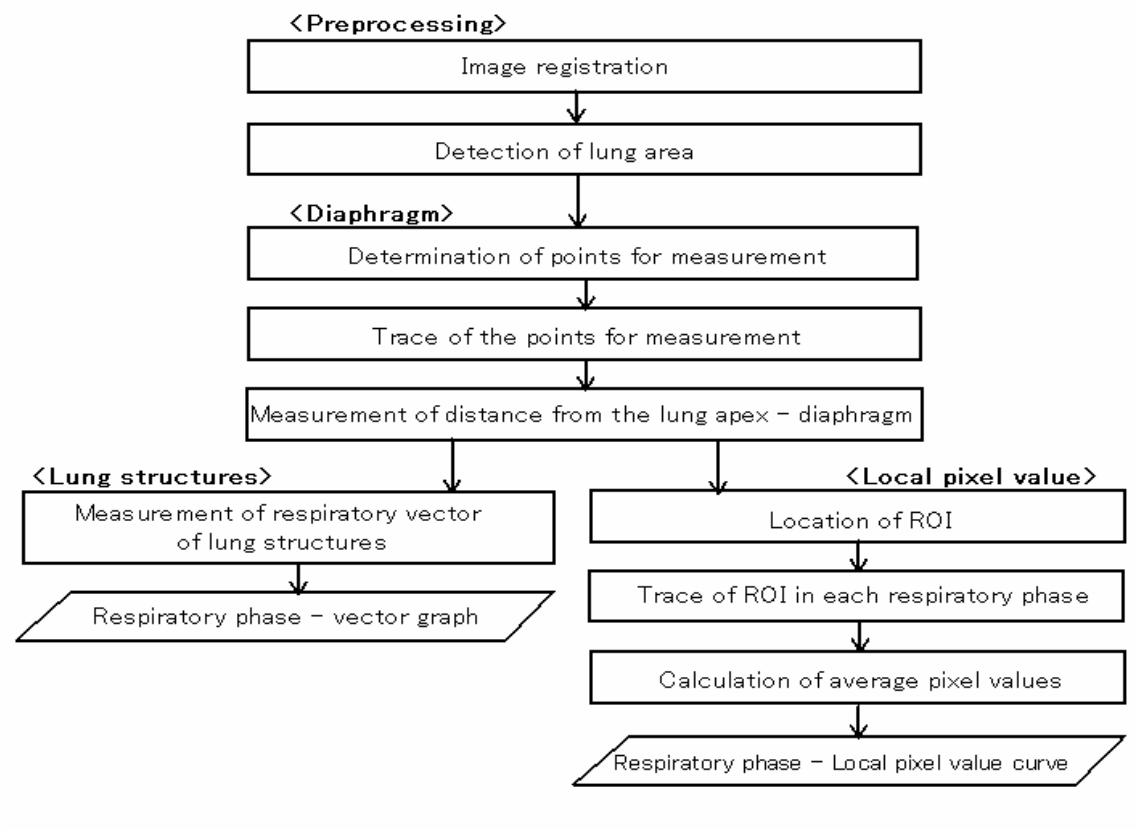

Fig. 1

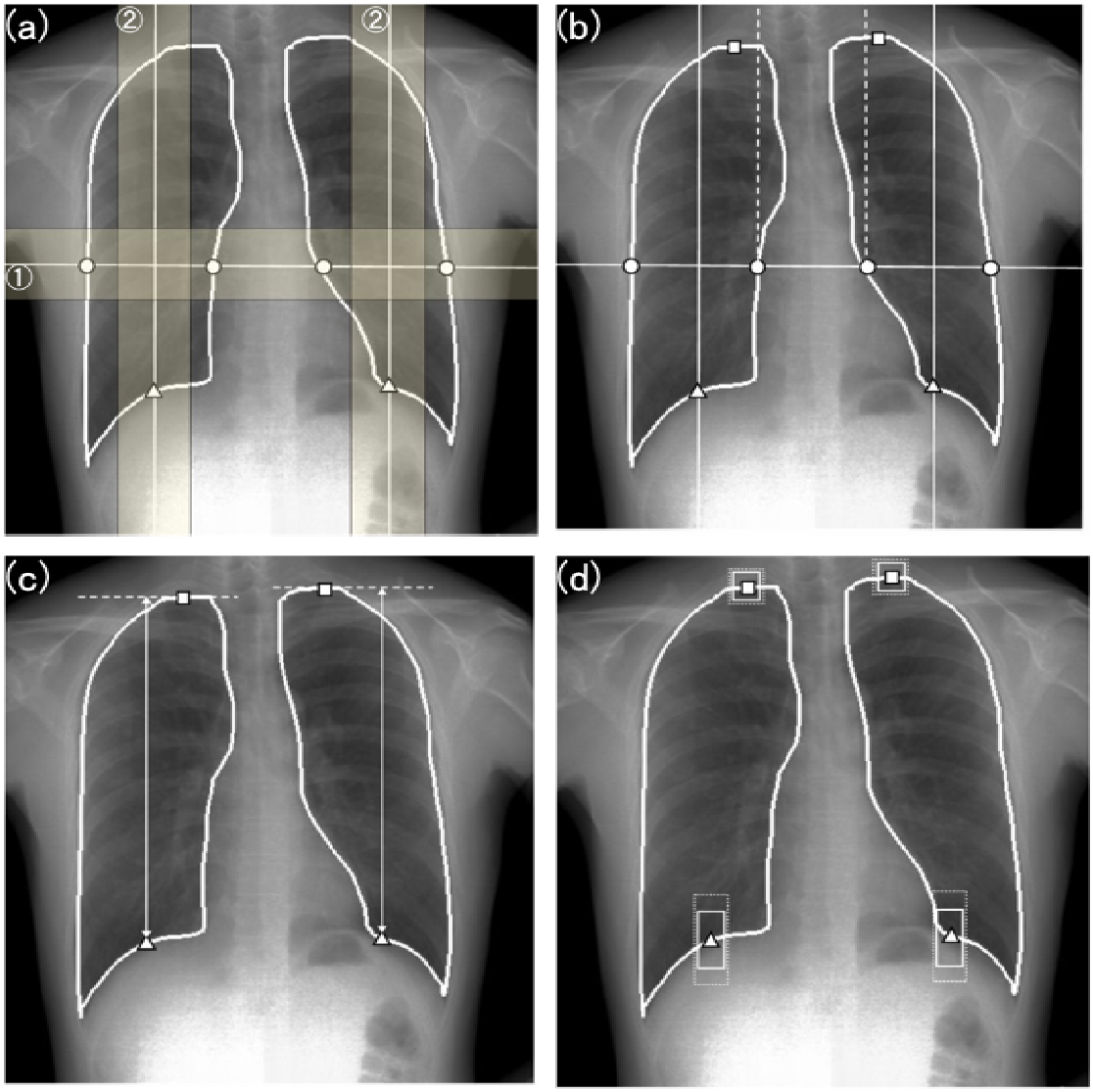

Fig. 2

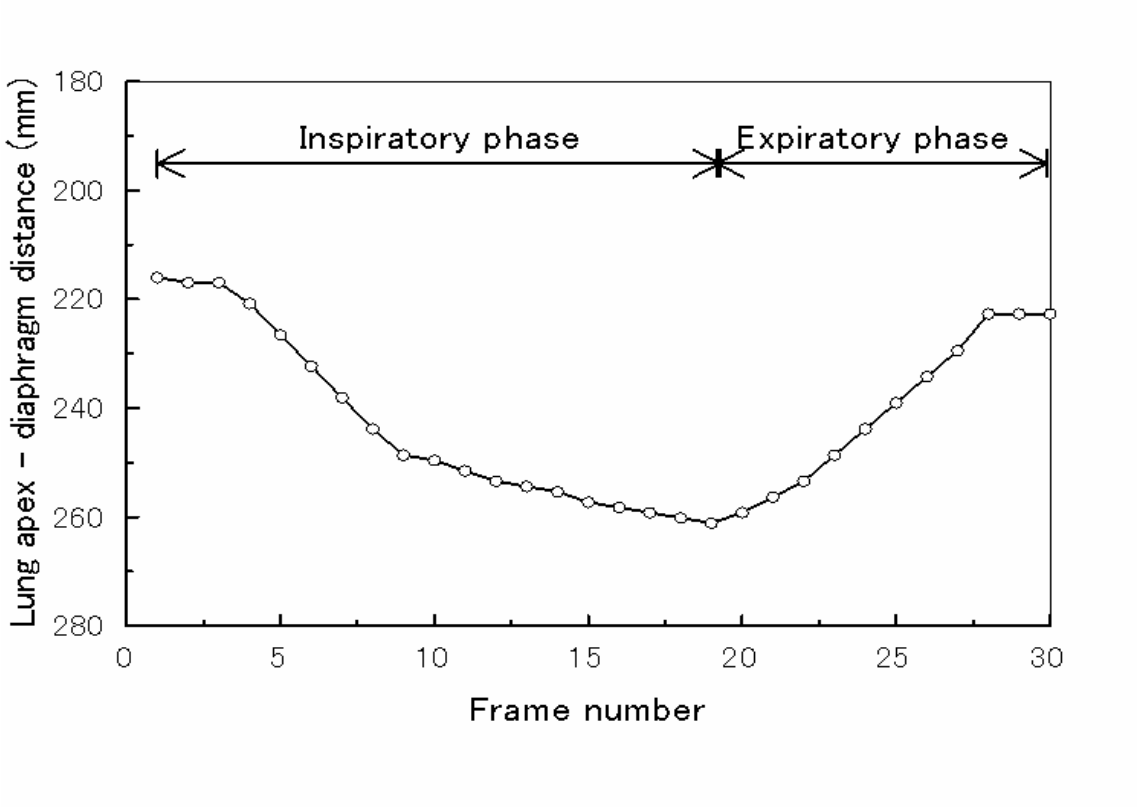
Inspiratory phase
Expiratory phase
Lung apex – diaphragm distance (mm)
180
200
220
240
260
280
0
5
10
15
20
25
30
Frame number

Fig. 3

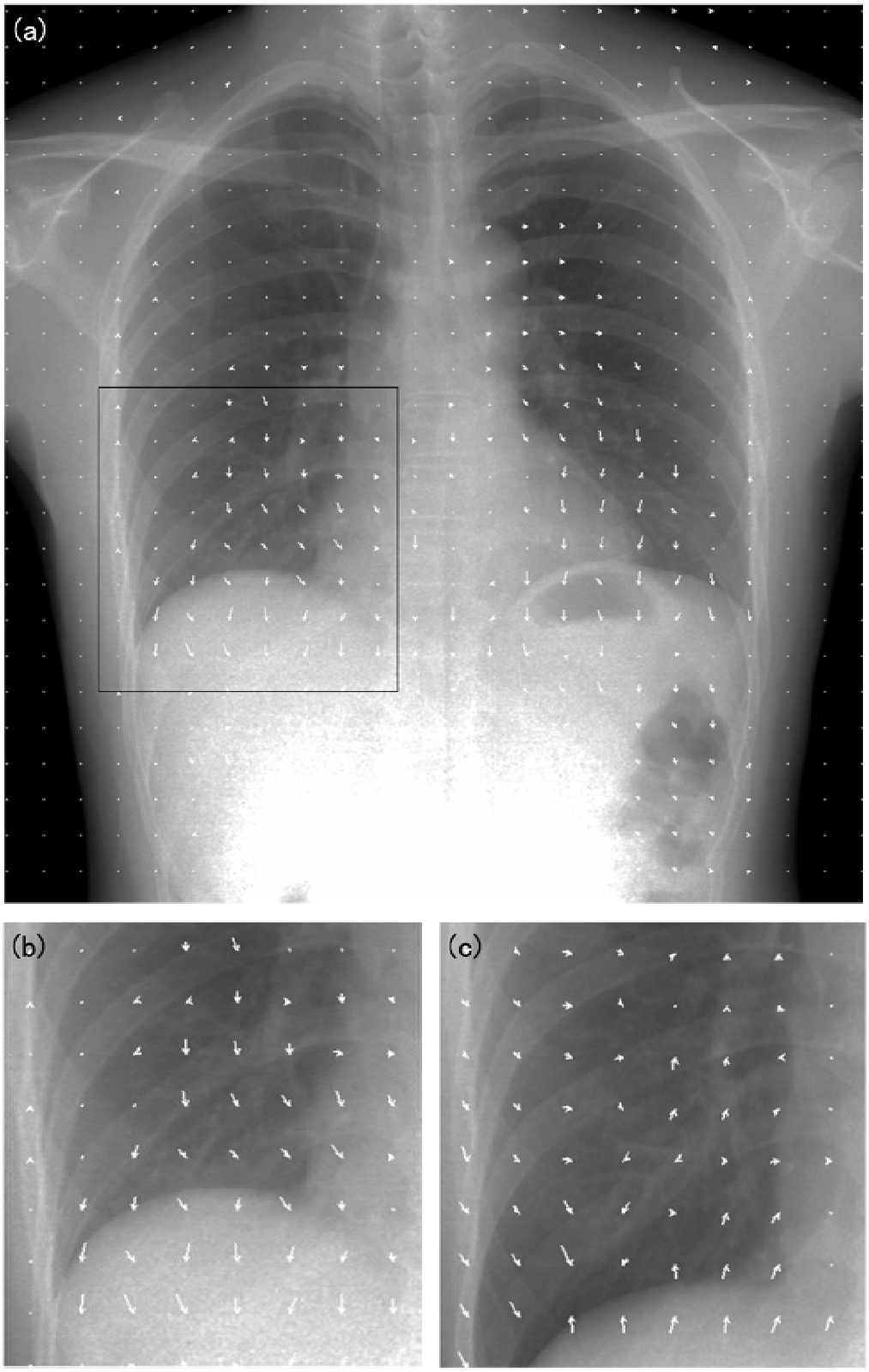

Fig. 4

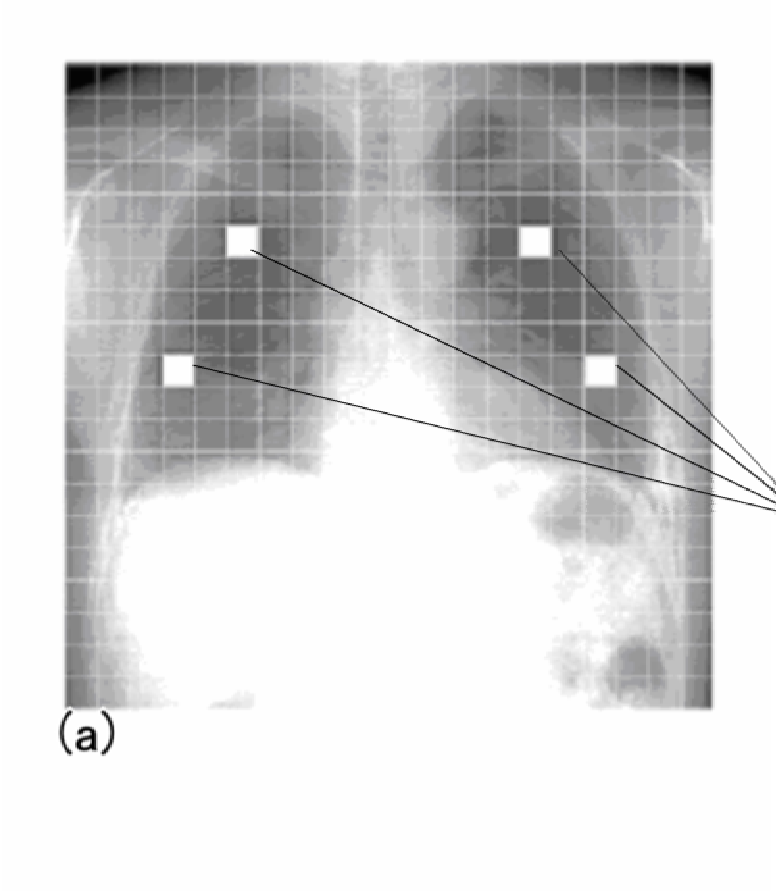

Fig. 5a

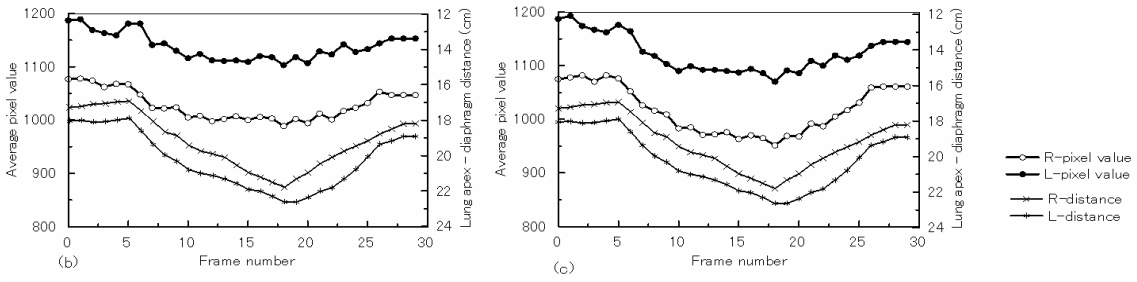

Fig.5bc

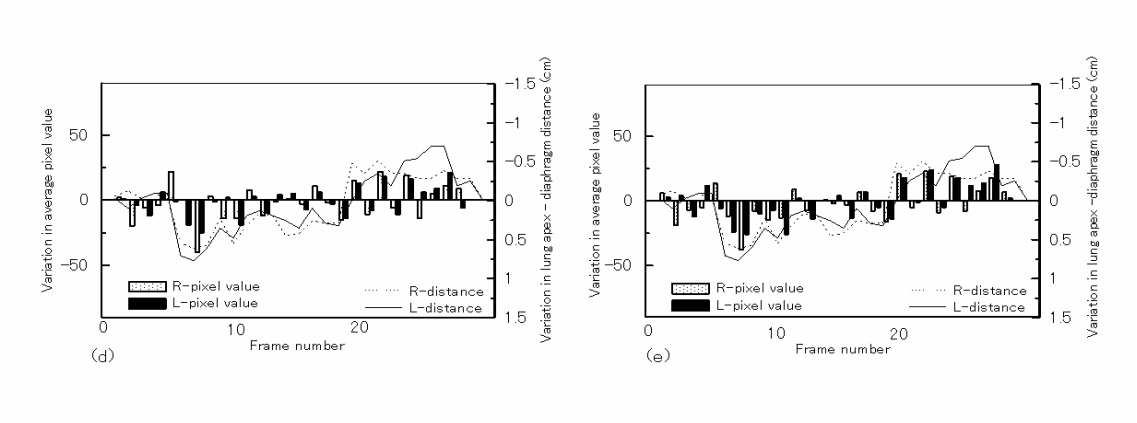
Variation in average pixel value
50
0
−50
−1.5
−1
−0.5
0
0.5
1
1.5
Variation in lung apex – diaphragm distance (cm)
R-pixel value
L-pixel value
R-distance
L-distance
0
10
20
Frame number
(d)
(e)

Fig. 5de

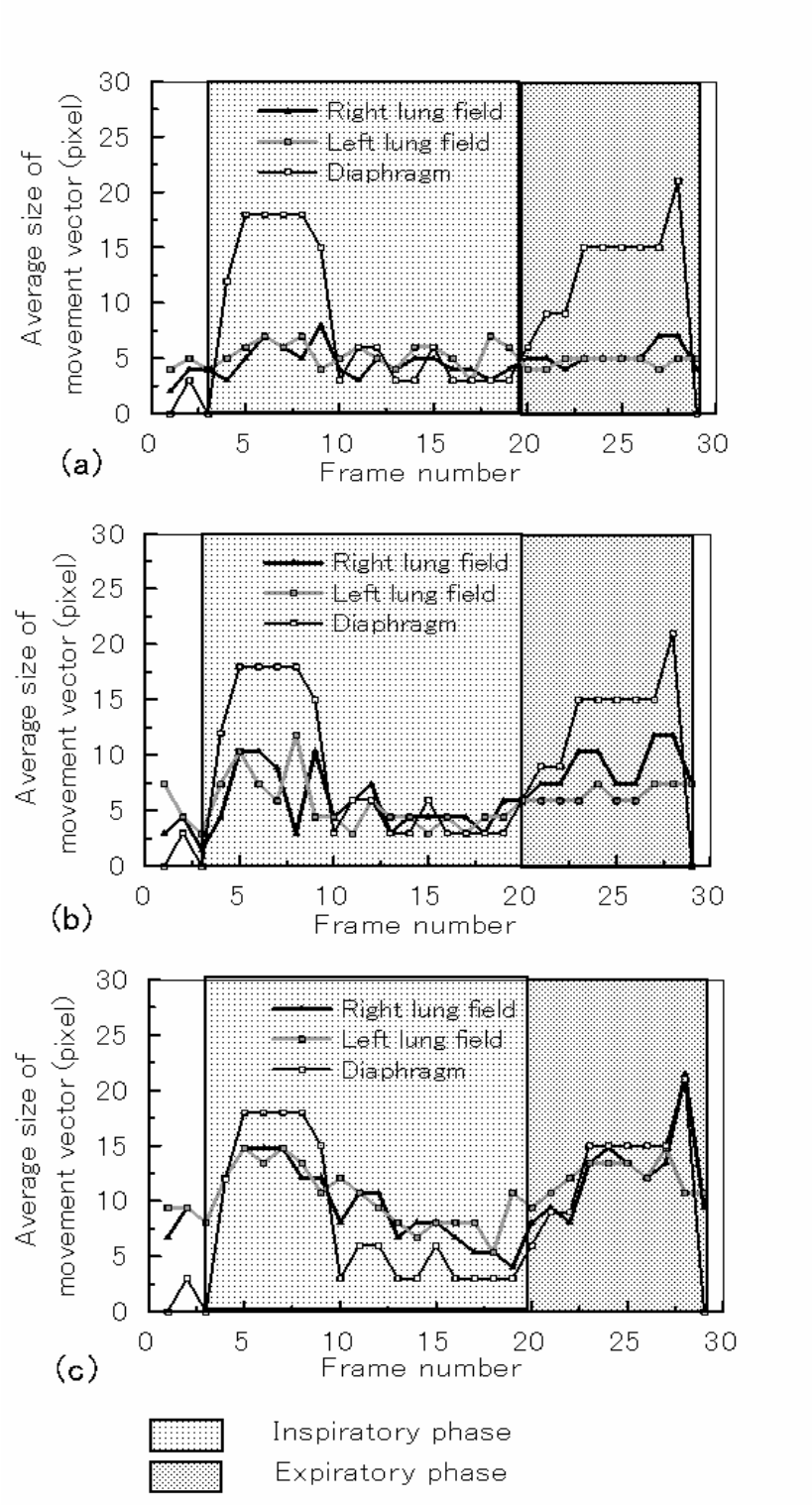
Average size of movement vector (pixel)
Right lung field
Left lung field
Diaphragm
Frame number
(a)
(b)
(c)
Inspiratory phase
Expiratory phase

Fig. 6

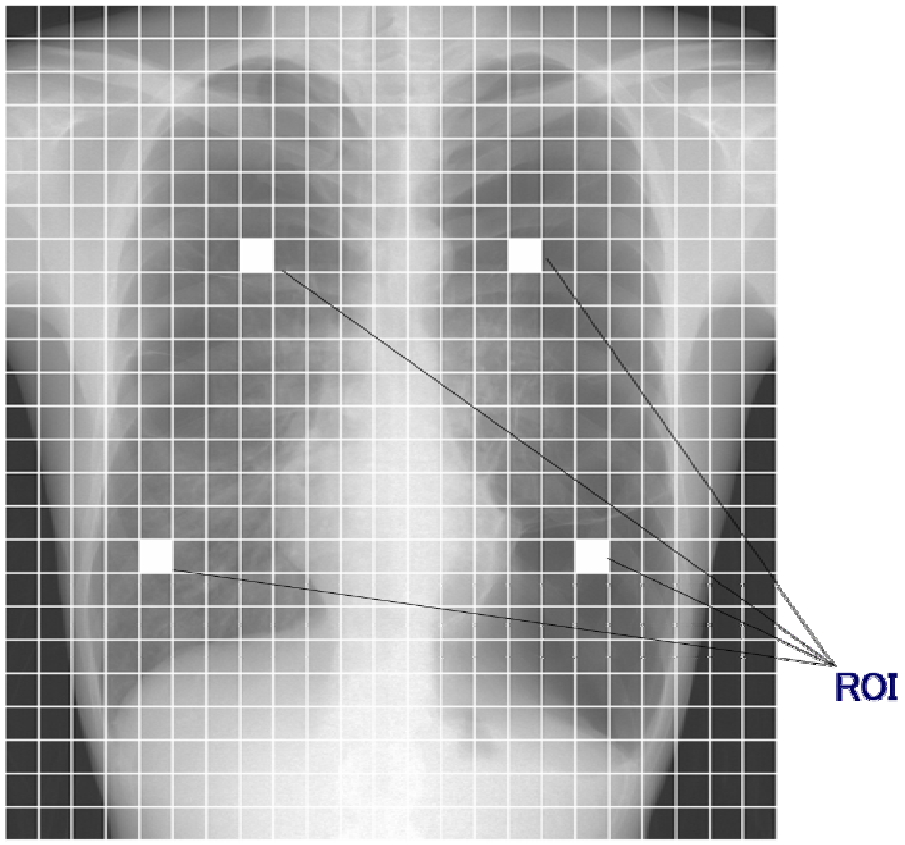

Fig. 7a

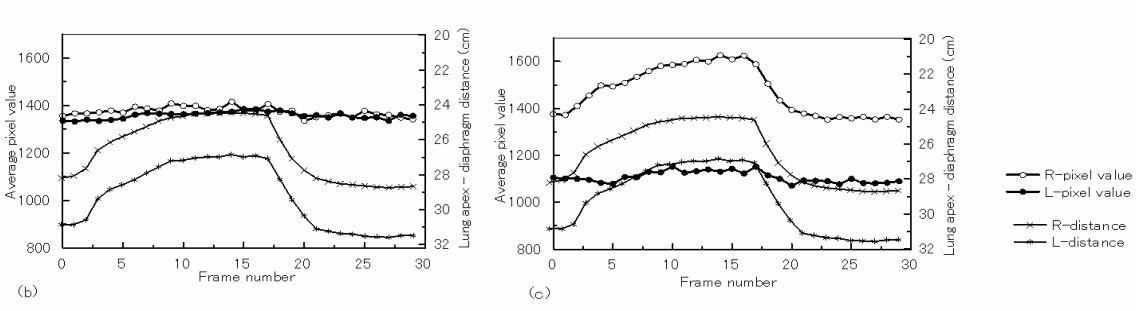

Fig. 7bc

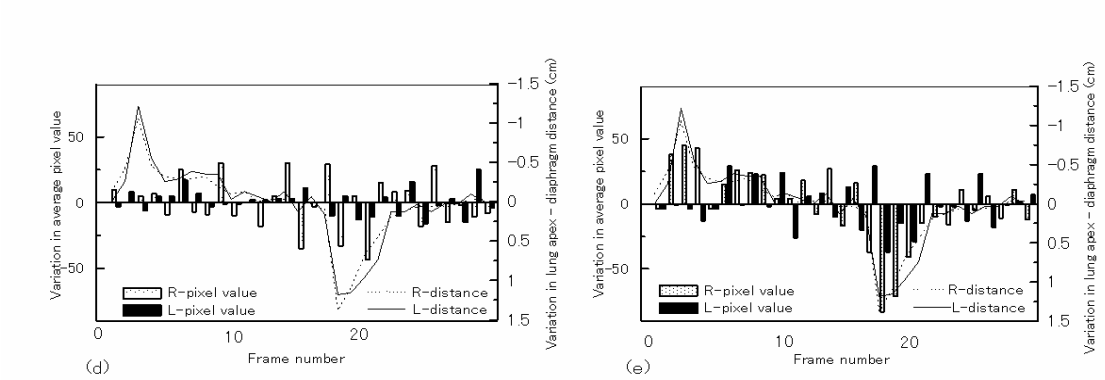
Variation in average pixel value
50
0
-50
-1.5
-1
-0.5
0
0.5
1
1.5
Variation in lung apex - diaphragm distance (cm)
R-pixel value
L-pixel value
R-distance
L-distance
0
10
20
Frame number
(d)
(e)

Fig. 7de

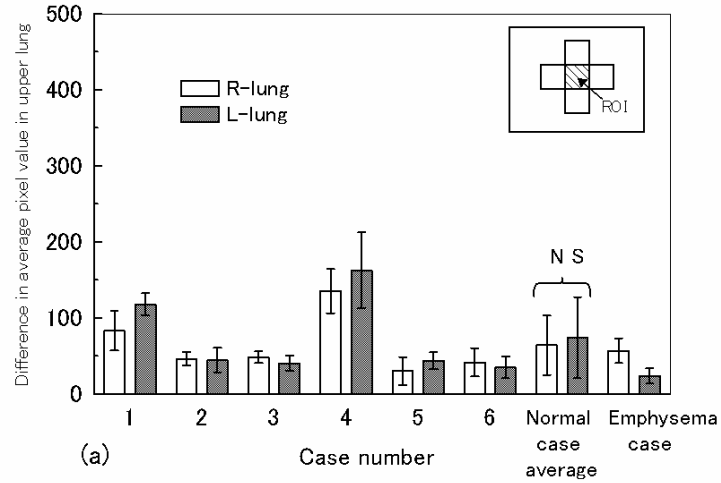
Difference in average pixel value in upper lung
500
400
300
200
100
0
R-lung
L-lung
ROI
N S
1
2
3
4
5
6
Normal case average
Emphysema case
(a)
Case number

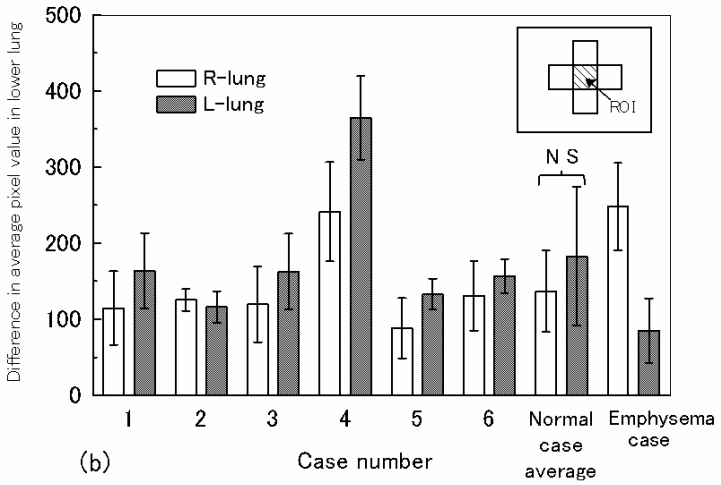
Difference in average pixel value in lower lung
500
400
300
200
100
0
R-lung
L-lung
ROI
N S
1
2
3
4
5
6
Normal case average
Emphysema case
(b)
Case number

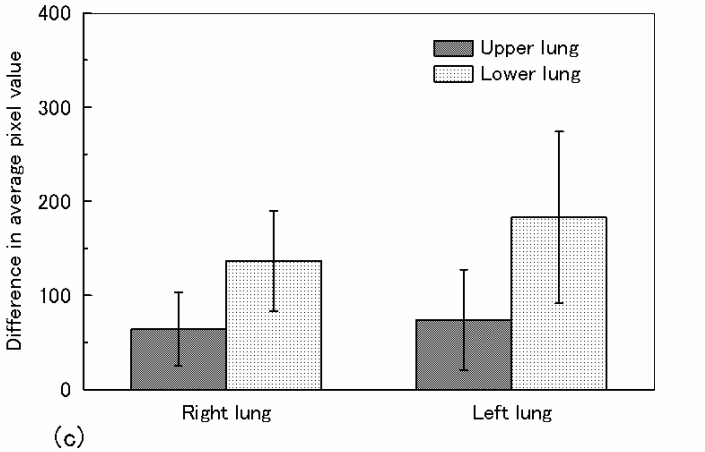
Difference in average pixel value
400
300
200
100
0
Upper lung
Lower lung
Right lung
Left lung
(c)

Fig. 8